BACCHUS

Impact of Biogenic versus Anthropogenic emissions on Clouds and Climate: towards a Holistic UnderStanding

Collaborative Project

SEVENTH FRAMEWORK PROGRAMME
ENV.2013.6.1-2

Atmospheric processes, eco-systems and climate change

Grant agreement no: 603445

Deliverable number:	**D3.5**
Deliverable name:	Global assessment of aerosol-cloud interactions with evaluated ESMs
WP number:	3
Delivery date:	Project month 54
Actual date of submission:	31/05/2018
Dissemination level:	PU
Lead beneficiary:	UOXF
Responsible scientist:	Philip Stier (UOXF)
Estimated effort (PM):	17.5
Contributor(s):	Duncan Watson-Parris (UOXF), Laurent Labbouz (UOXF), Haochi Che (UOXF), David Neubauer (ETHZ), Ulrike Lohmann (ETHZ), Risto Makkonen (UHEL), Moa Sporre (UIO).
Estimated effort contributor(s) (PM):	UOXF: 10PM plus 4PM unfunded; ETHZ: 2PM (unfunded); UHEL: 1PM (unfunded); UIO: 0.5PM
Internal reviewer:	Ulrike Lohmann

1. Executive summary

Deliverable 3.5 provides a global assessment of aerosol-cloud interactions with the BACCHUS ESMs that have been evaluated in deliverable 3.4. Specifically, this deliverable focuses on the response of clouds, precipitation and the global radiation balance to anthropogenic aerosol perturbations in the following ESMs: MPI-ESM-HAM (here referred to by its atmospheric component ECHAM-HAM), MPI-ESM-HAM-CCFM (a modified version of MPI-ESM-HAM, including the convective cloud field model and explicit aerosol-convection coupling, HadGEM-UKCA (in a version corresponding to a UKESM1 prototype) as well as NorESM.

Highlights

- The BACCHUS ESMs show a distinct increase in the liquid water path of about 6-7% to anthropogenic aerosol perturbations. Strong increases in LWP to aerosol perturbations have been linked to excessive aerosol radiative forcing [*Malavelle et al.*, 2017; *Quaas et al.*, 2009] so this distinct LWP response in current state-of-the-art models will require further attention.
- The precipitation response to aerosol perturbations is variable across models. Nonetheless, some precipitation response patterns are consistent, in particular the decrease of precipitation over large parts of China and a general reduction in precipitation over large parts of central Africa.
- The BACCHUS ESMs simulate relative model diversity in the direct aerosol radiative effects, often considered to be well understood, that exceeds the diversity in the indirect radiative effects. Nonetheless, the absolute diversity is larger for the indirect radiative effects. This is true in the global mean but also in the regional response patterns. This can likely be attributed to the strong sensitivity of direct forcing to aerosol absorption, which modulates the sign of the top-of-atmosphere forcing. Resulting available global-mean all-sky direct radiative forcings range from -0.37Wm^{-2} (HadGEM-UKCA) to +0.10Wm^{-2} (ECHAM-HAM-CCFM).
- The BACCHUS ESMs simulate total aerosol effective radiative forcing (ERF) forcing ranging from -0.96Wm^{-2} (ECHAM-HAM) to -1.59Wm^{-2} (HadGEM-UKCA). It is likely that these relatively strong ERFs are driven by strong increases in cloud liquid water. Fundamental research on related cloud and aerosol processes remains a key priority for reducing the uncertainty in the total anthropogenic perturbation of the climate system.

2. Models

MPI-ESM-HAM (here referred to by its atmospheric component ECHAM-HAM) is a global aerosol climate model, used in its version ECHAM6.3-HAM2.3 [*Stier et al.*, 2005; *Stier et al.*, 2007; *Tegen et al.*, 2018; *Zhang et al.*, 2012]. It consists of the general circulation model ECHAM6 [*Stevens et al.*, 2013] coupled to the latest version of the aerosol module HAM2 and uses a two-moment cloud microphysics scheme that includes prognostic equations for the cloud droplet and ice crystal number concentrations as well as cloud water and cloud ice [*Lohmann et al.*, 2007]. An empirical cloud cover scheme [*Sundqvist et al.*, 1989] is used to compute stratiform cloud cover. The autoconversion of cloud droplets to rain follows [*Khairoutdinov and Kogan*, 2000]. Cumulus convection is represented by the parameterization of *Tiedtke* [1989] with modifications by *Nordeng* [1994] for deep convection. ECHAM-HAM is coupled to Max Planck Institute Ocean Model (MPIOM) [*Jungclaus et al.*, 2013] and the Hamburg Ocean Carbon Cycle Model (HAMOCC) [*Ilyina et al.*, 2013] in MPI-ESM-HAM. In these simulations only the atmospheric model ECHAM-HAM is used (ECHAM-HAM REF)

MPI-ESM-HAM-CCFM is an extended version of MPI-ESM-HAM, replacing the default mass-flux convection parameterisation by *Tiedtke* [1989] and [*Nordeng*, 1994] with the convective cloud field model CCFM [*Wagner and Graf*, 2010]. CCFM represents a spectrum of convective clouds with different properties (vertical velocity, microphysical properties, …) within each ECHAM-HAM grid-box and provides explicit aerosol-convection coupling [*Kipling et al.*, 2017; *Labbouz et al.*, 2018]. The improved representation of the convective cloud spectrum in MPI-ESM-HAM-CCFM has been evaluated as part of BACCHUS D3.2, as published in *Labbouz et al.* [2018].

HadGEM-UKCA is the atmospheric component of the UKESM1 ESM used in a prototype version of UKESM1. Coupled within the climate model, the aerosol-chemistry model UKCA uses components of HadGEM3 for the large-scale advection, convective transport, and boundary layer mixing of its chemical tracers. Advection is semi-Lagrangian with conservative and monotone treatment of tracers. Convective transport is treated according to the mass-flux scheme of *Gregory and Rowntree* [1990] and is applicable to moist convection of all types (shallow, deep, and mid-level) in addition to dry convection. For boundary layer mixing, UKCA uses a boundary layer turbulent mixing scheme which includes a representation of non-local mixing in unstable layers and an explicit entrainment parameterisation. The aerosol model of UKCA, GLOMAP-Mode [*Mann et al.*, 2010] is conceptually similar to the M7 model [*Vignati et al.*, 2004] used by HAM in MPI-ESM.

NorESM, the Norwegian Earth System Model [*Bentsen et al.*, 2013] is based on the CESM model but uses a different ocean model (MICOM) and a different aerosol scheme in the atmospheric model CAM. The aerosol scheme in the NorESM version of CAM, called CAM- Oslo, can be described as an aerosol life cycle scheme which calculates production tagged mass concentrations of different aerosol species [*Kirkevåg et al.*, 2018]. In the current simulations the NorESM model was run with the CAM-Oslo version 5.3, which is configured with the microphysical two moment scheme MG1.5 [*Gettelman and Morrison*, 2015; *Morrison and Gettelman*, 2008] for stratiform clouds. The scheme includes prognostic equations for cloud liquid water (mass and number) and ice (mass and number) and a version of the [*Khairoutdinov and Kogan*, 2000] autoconversion scheme where subgrid variability of cloud water has been included. CAM5.3-Oslo has a shallow convection scheme [*Park and Bretherton*, 2009] and a deep convection scheme [*Zhang and Mcfarlane*, 1995].

3. Simulation setup

All models were set up to isolate anthropogenic aerosol effects on the global radiation balance and climate. Both the NorESM and ECHAM-HAM-REF results are averages from free-running 20-year simulations, while the ECHAM-HAM-CCFM and HadGEM-UKCA runs are averaged from simulations nudged to ERA-Interim re-analysis for the year 2008 (after spin-up). Model resolutions were corresponding to typical ESM setups (ECHAM-HAM(-CCFM): T63/L31 corresponding to 1.875°x1.875°; HadGEM: N96/L38, corresponding to 1.25°x1.875°; NorESM: 1.9°x2.5°). All models use observed sea surface temperatures and sea ice cover. Two simulations were done by each model, one with pre-industrial (PI) and one with present-day (PD) aerosol emissions but otherwise identical simulation setup.

The effect of ice nuclei on cloud properties and its representation in global models was discussed in Deliverable 2.4 and has not been repeated in this deliverable.

4. Results

Figure 1 shows the total aerosol burdens for each model for pre-industrial (PI) and present-day (PD) aerosol emissions as well as the PD-PI difference. As expected, total aerosol burdens are heavily dominated by the global dust distribution. However, the PD-PI changes reveal the pattern of anthropogenic perturbations, corresponding to key anthropogenic emission regions, such as Asia, as well as biomass burning regions, such as central Africa. The large variability in the ECHAM-HAM simulations can be attributed to the high variability of dust emissions in the free running ECHAM6.3-HAM2.3 simulation - a 90% difference in dust burden can occur form one year to the next.

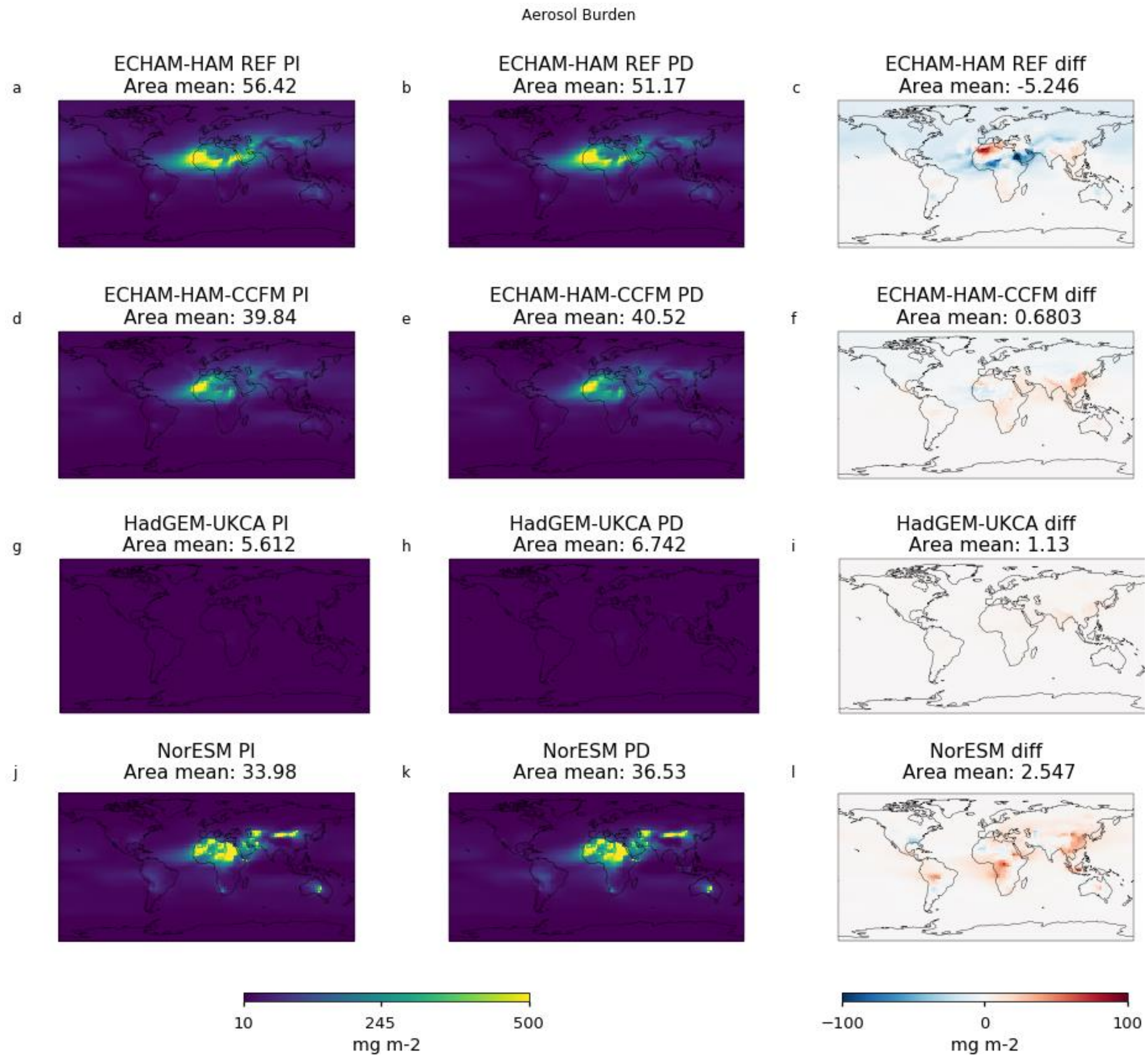

Figure 1: Total aerosol burden for each model in both pre-industrial (PI) and present day (PD) conditions, and the difference. *Please note that dust in this version of HadGEM-UKCA is treated by a bin model, separately from GLOMAP-mode, and therefore does not contribute to the diagnosed GLOMAP aerosol burdens.*

The total aerosol optical depth (AOD) for each model for PI, PD and the PD-PI difference is shown in Figure 2. HadGEM-UKCA shows the largest PD-PI difference of the models shown here, and the differences are more spatially extended than the other models. The ECHAM-HAM reference simulation has the weakest global-mean AOD change, partly due to a decrease in Saharan dust between the PI and PD. This is also reflected in the aerosol burdens discussed above.

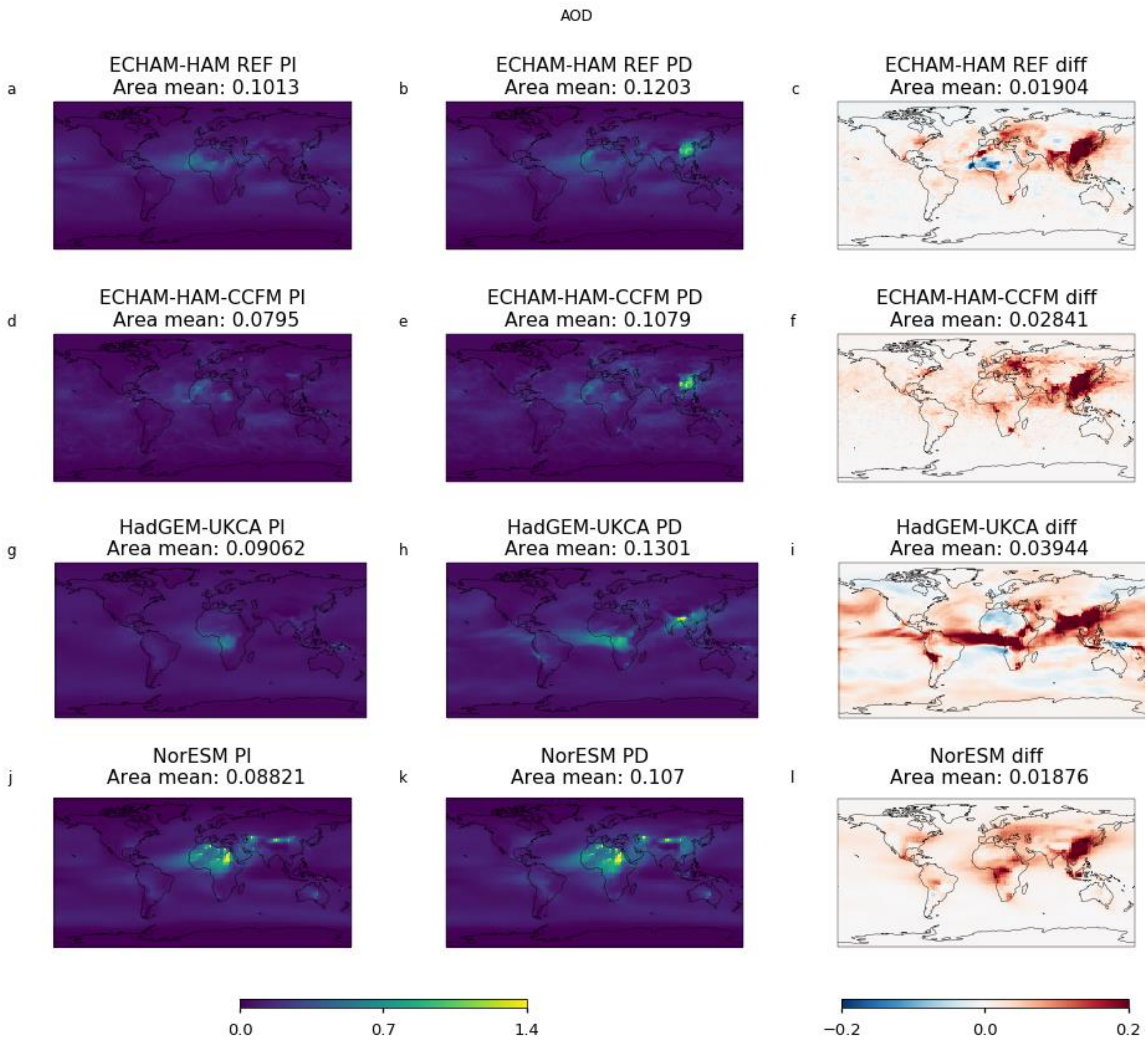

Figure 2: Aerosol optical depth (AOD) at 550nm for each model in both pre-industrial (PI) and present day (PD) conditions, and the difference.

The cloud liquid water path for PI and PD simulations and the PD-PI difference corresponding to the anthropogenic effect is shown in Figure 3. All models show a positive LWP response to anthropogenic aerosols in the northern Oceans, downwind of major source areas. It is worth noting that both ECHAM-HAM models largely agree on the LWP response pattern, despite the use of entirely different convection parameterisations and active aerosol convection interactions in ECHAM-HAM-CCFM. However, regional patterns differ significantly across models: both ECHAM-HAM versions as well as NorESM show a strong LWP response in the anthropogenic source regions that differs from HadGEM-UKCA. Strong increases in liquid water path to aerosol perturbations may not be consistent with observations [*Quaas et al.*, 2009] and have been linked to excessive aerosol radiative forcing [*Malavelle et al.*, 2017] so this distinct difference in the liquid water path response in current state-of-the-art models will require further attention.

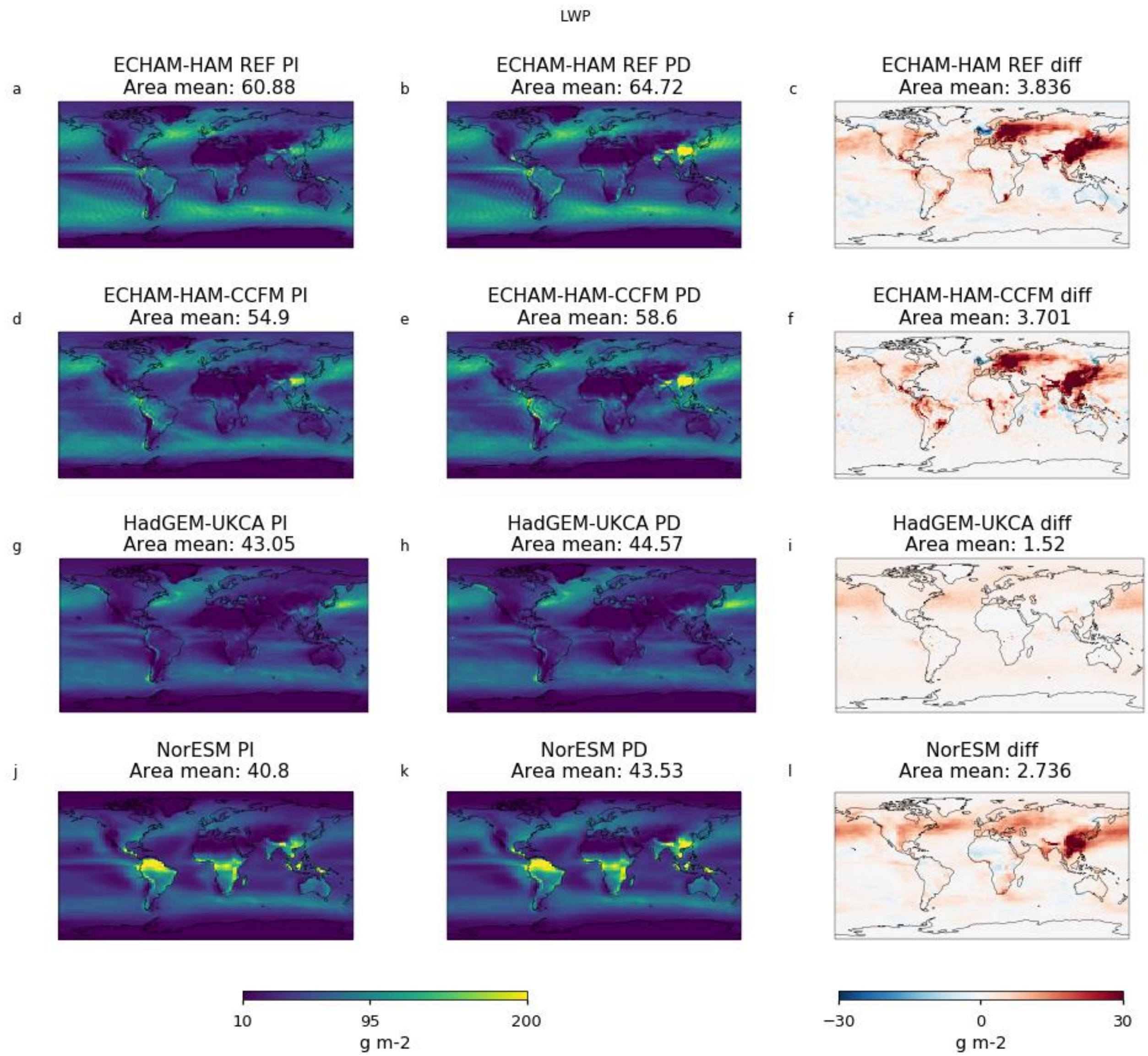

Figure 3: Cloud liquid water path (LWP) for each model in both pre-industrial (PI) and present day (PD) conditions, and the difference.

Changes in ice water path (IWP) from pre-industrial to present day times (Figure 4) are at least two orders of magnitude smaller than changes in LWP and primarily related to chaotic noise between the PI and PD simulations. This is not unexpected due to the fact that the effect of ice nuclei on cloud properties has not been included in model simulations, except for ECHAM-HAM, where BC particles act as IN – but ECHAM-HAM is insensitive to heterogeneous freezing in mixed-phase clouds. The HadGEM-UKCA IWP is significantly larger than the IWP of the other ESMs. However, it is worth noting that the global IWP is highly uncertain due to the lack of reliable observational constraints. Hence, the IWP of the BACCHUS ESMs lies well within the (wide) envelope of current climate models and the observational uncertainty [*Li et al.*, 2016; *Waliser et al.*, 2009].

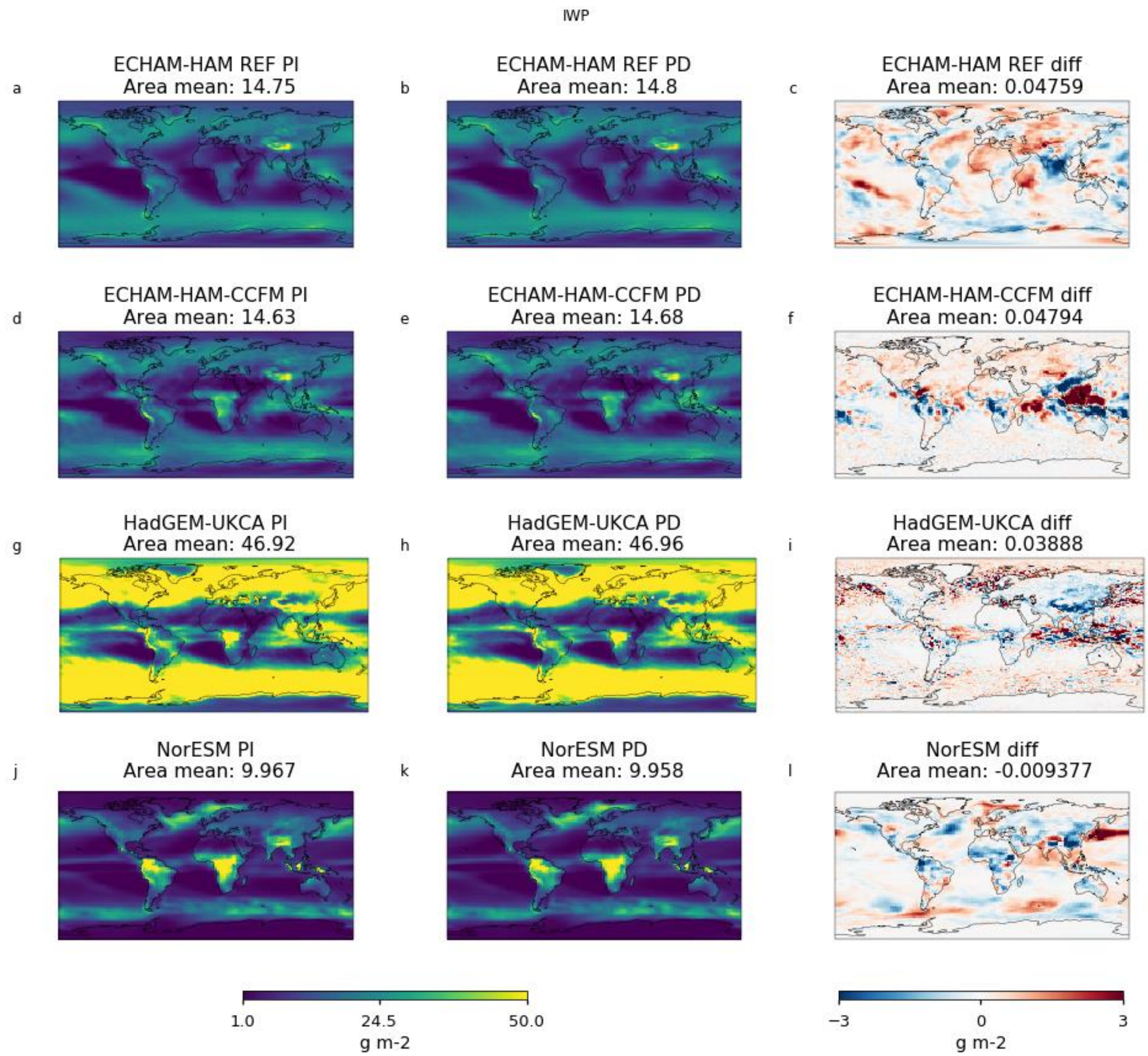

Figure 4: Cloud ice water path (IWP) for each model in both pre-industrial (PI) and present day (PD) conditions, and the difference.

Global patterns of precipitation, shown Figure 5, are consistent across models with small global mean changes from PI to PD, as can be expected from energetic constraints on precipitation [*Allen and Ingram*, 2002; *Muller and O'Gorman*, 2011]. The PD-PI precipitation response pattern remains noisy, in particular for the shorter ECHAM-HAM-CCFM and HadGEM-UKCA simulations. Nonetheless, some precipitation response patterns are consistent across all models, in particular the decrease of precipitation over large parts of China and a general reduction in precipitation over large parts of central Africa. Interestingly, precipitation changes in HadGEM-UKCA are significantly smaller outside the tropics than in any of the other models.

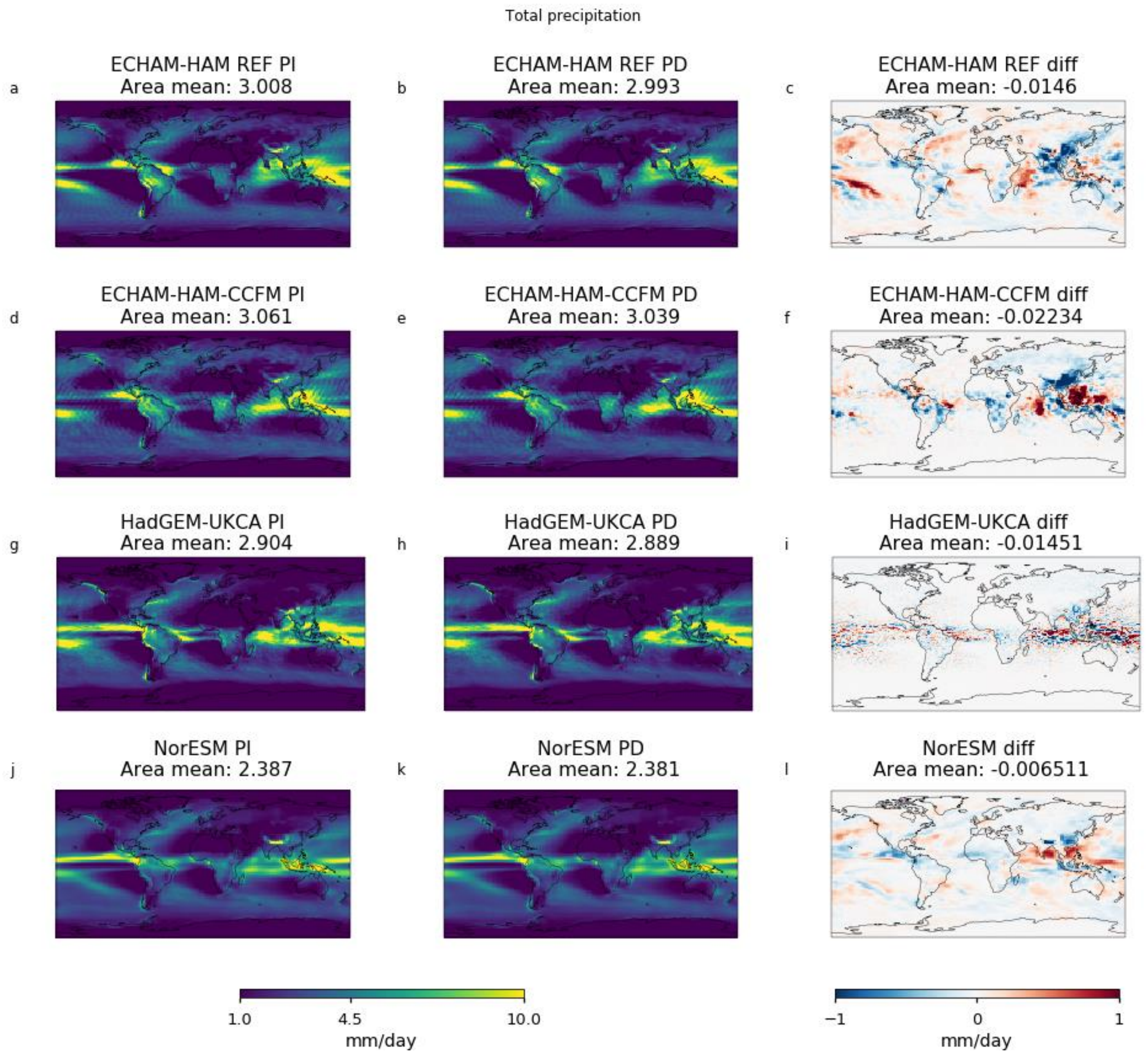

Figure 5: Total precipitation (convective plus stratiform) for each model in both pre-industrial (PI) and present day (PD) conditions, and the difference.

By making two separate radiation calls during the model simulation, one which includes the radiative interaction of aerosols and one without, it is possible to diagnose the total instantaneous direct aerosol radiative effect from each model. Figure 6 show the clear-sky instantaneous aerosol radiative effect and the PD-PI difference, which is instantaneous anthropogenic aerosol radiative forcing ($RF_{ari\ clear\text{-}sky}$), in each model. Models simulate a consistent patterns of negative direct clear-sky forcings, with maxima over the anthropogenic source region in Asia, Europe and the US. However, there remain large differences in the magnitude of the radiative effects and anthropogenic forcing between the models with $RF_{ari\ clear\text{-}sky}$ ranging from -0.27 Wm^{-2} in ECHAM-HAM-REF to -1.01 Wm^{-2} in HadGEM-UKCA.

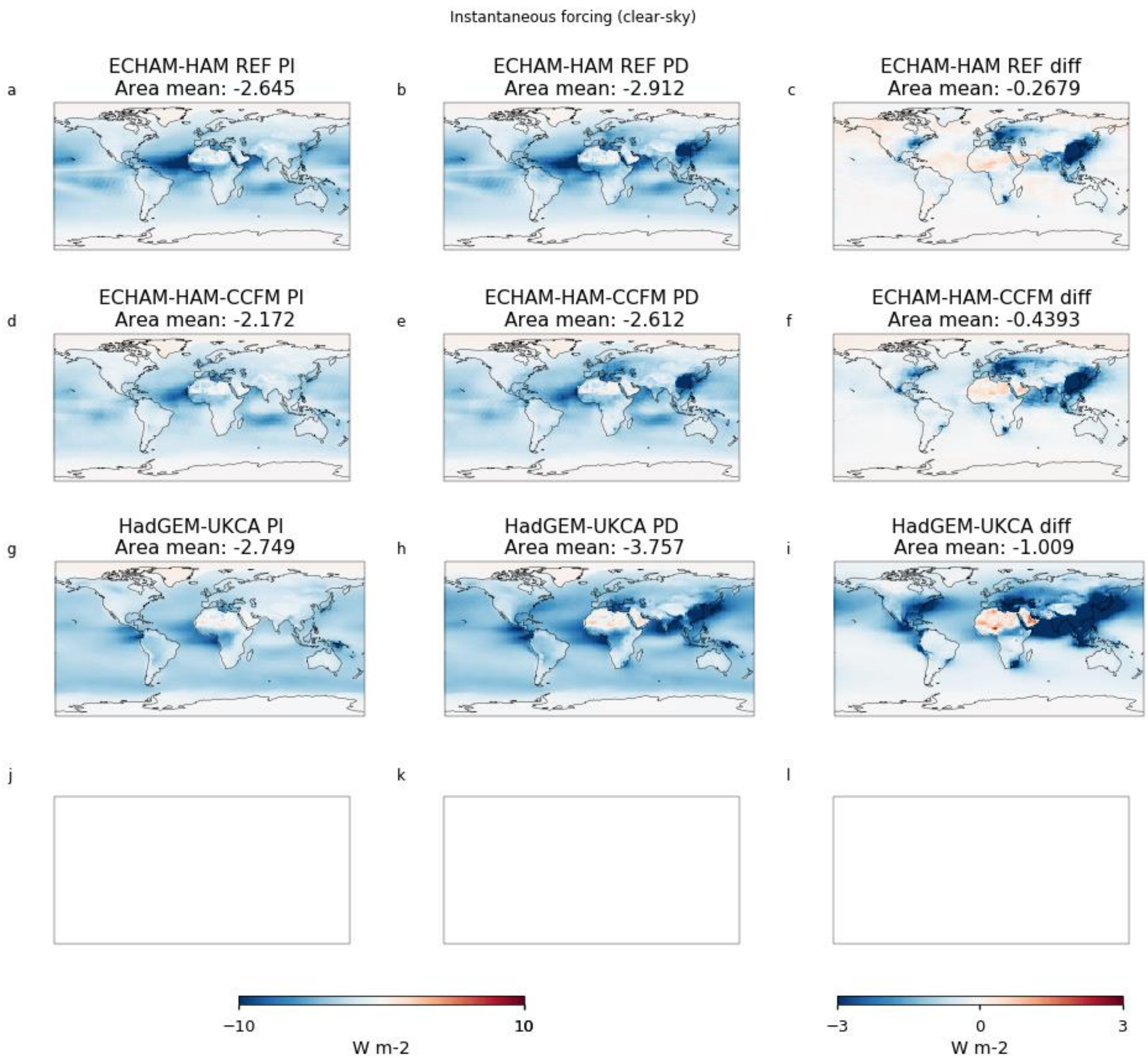

Figure 6: Instantaneous aerosol effect under clear-sky conditions for each model in both pre-industrial (PI) and present day (PD) conditions, and the resulting forcing. *Instantaneous radiative effect fields are not available for NorESM.*

The all-sky instantaneous aerosol direct radiative effect and the PD-PI difference, which is the instantaneous all-sky anthropogenic aerosol radiative forcing ($RF_{ari\ all\text{-}sky}$), for each model is shown in Figure 7. Across models, the all-sky instantaneous radiative effect and $RF_{ari\ all\text{-}sky}$ is significantly more positive than the clear-sky effects. This is due to the higher effective albedo of the surface underlying the aerosol layers [*Haywood and Shine*, 1995] as well as due to cloud masking of the clear-sky predominantly negative aerosol radiative effects. All models show a large positive forcing associated with biomass burning aerosol above the South-East Atlantic stratocumulus cloud deck, however, the magnitude of the effect differs significantly across models and even between the two ECHAM-HAM model versions: ECHAM-HAM-CCFM shows the strongest response in this area, as well as over the Amazon. Consistent with its strongly negative clear-sky forcing, HadGEM-UKCA simulates a significantly stronger negative anthropogenic all-sky forcing, in particular over south-East Asia, where also corresponding AOD changes were large (c.f. Figure 2).

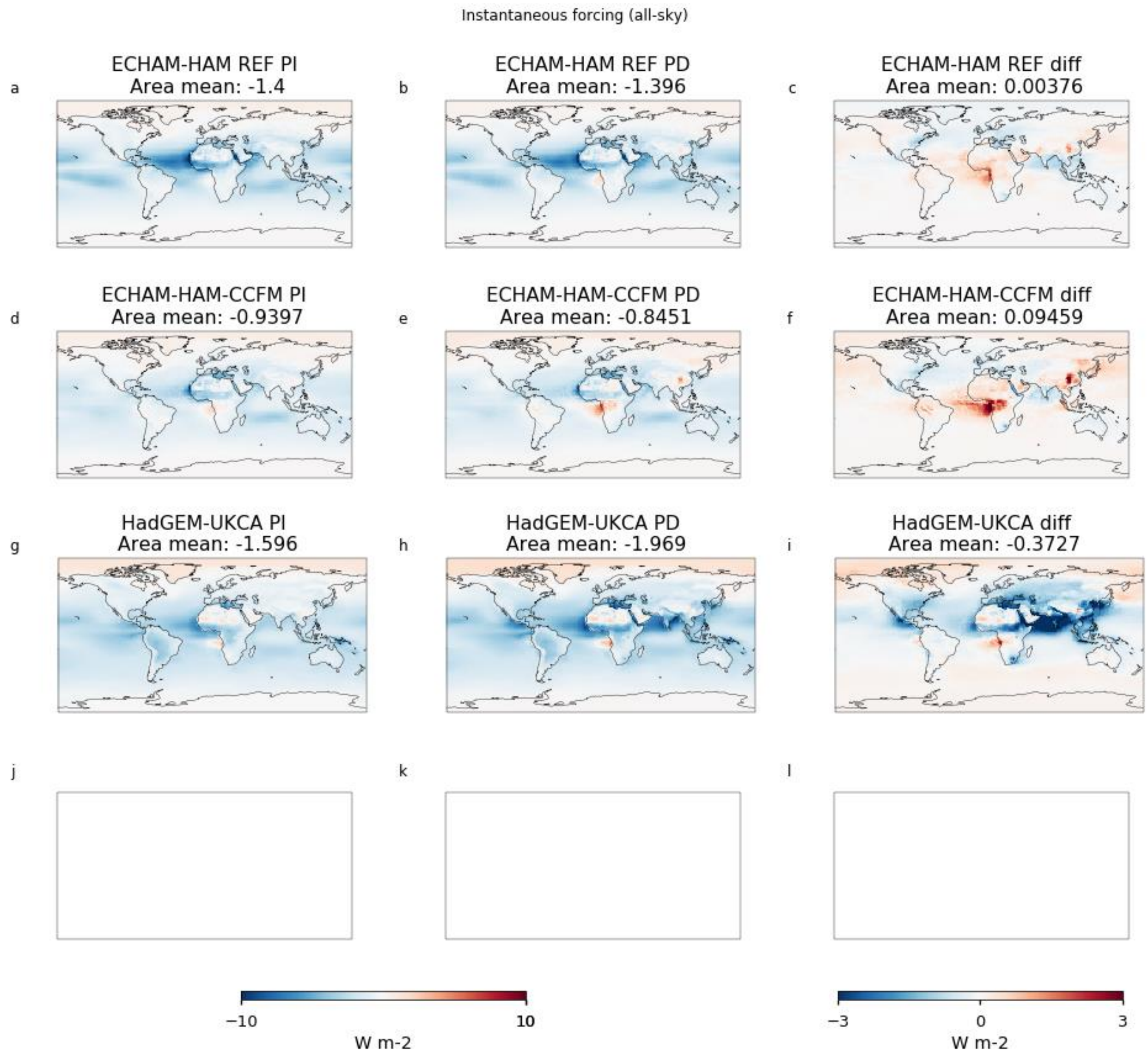

Figure 7: Instantaneous aerosol effect under all-sky conditions for each model in both pre-industrial (PI) and present day (PD) conditions, and the resulting forcing. *Instantaneous radiative effect fields are not available for NorESM.*

The total aerosol effective radiative forcing (ERF, allowing for fast adjustments) for all models is shown for clear-sky and all-sky conditions in Figure 8. Interestingly, models exhibit significantly larger diversity in the magnitude and patterns of the clear-sky ERF with global-mean clear-sky ERFs ranging from -0.08Wm^{-2} in ECHAM-HAM to -1.23Wm^{-2} simulated by HadGEM-UKCA.

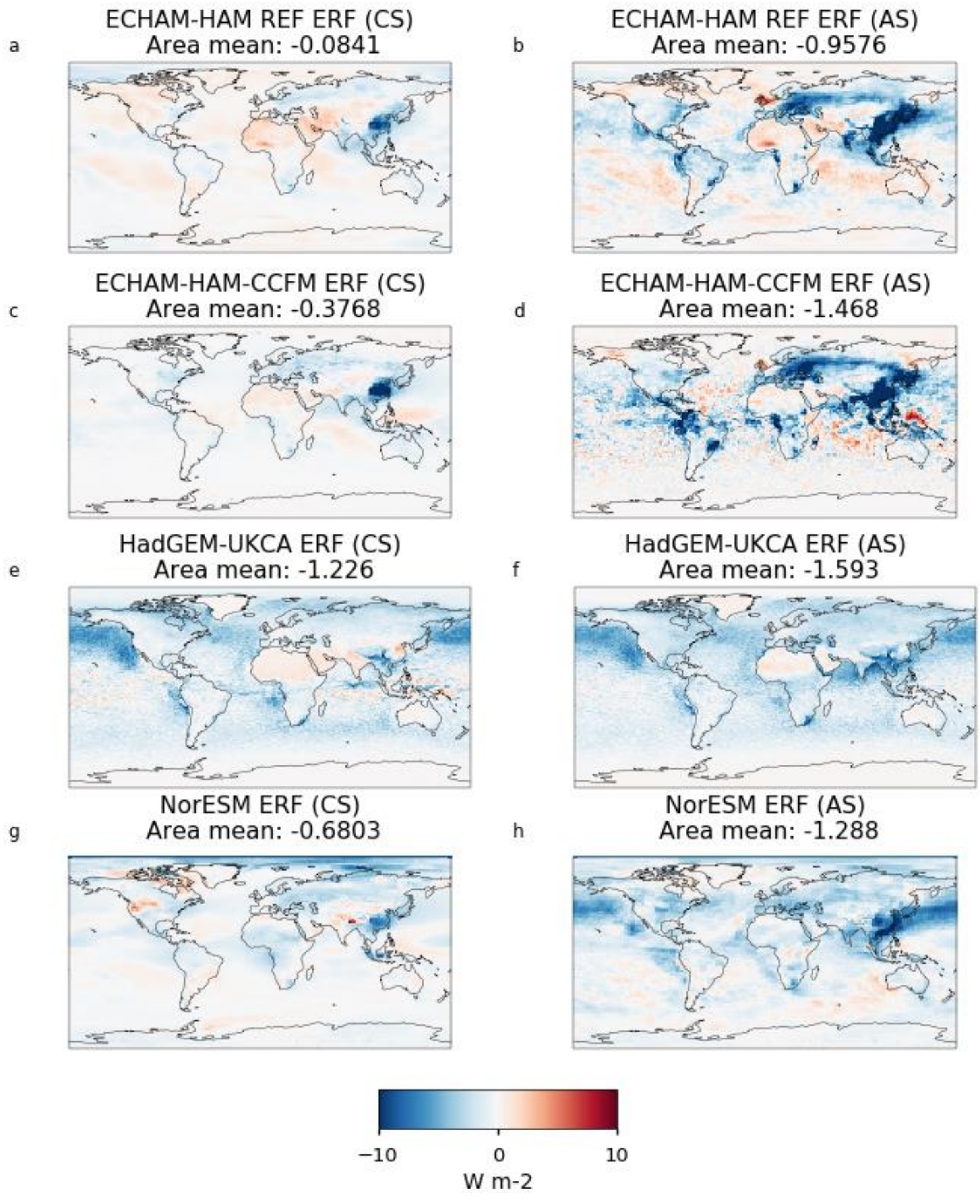

Figure 8: Total aerosol effective radiative forcing (ERF) for each model under clear- and all-sky conditions.

All-sky effective radiative forcings across models are surprisingly more consistent, ranging from -0.96Wm^{-2} in ECHAM-HAM to -1.59Wm^{-2} in HadGEM-UKCA with largely consistent patterns in the major anthropogenic outflow regions. The comparison of clear-sky ERF (Figure 8) with clear-sky RF (Figure 6) reveals the importance of fast-adjustments. For example, ECHAM-HAM aerosol effects change from -0.27Wm^{-2} to -0.08Wm^{-2} when allowing for fast adjustments, including semi-direct effects.

5. References

Allen, M. R., and W. J. Ingram (2002), Constraints on future changes in climate and the hydrologic cycle, Nature, 419(6903), 224-232 doi: doi:10.1038/nature01092.

Bentsen, M., I. Bethke, J. B. Debernard, T. Iversen, A. Kirkevag, O. Seland, H. Drange, C. Roelandt, I. A. Seierstad, C. Hoose, and J. E. Kristjansson (2013), The Norwegian Earth System Model, NorESM1-M - Part 1: Description and basic evaluation of the physical climate, Geosci Model Dev, 6(3), 687-720 doi: 10.5194/gmd-6-687-2013.

Gettelman, A., and H. Morrison (2015), Advanced Two-Moment Bulk Microphysics for Global Models. Part I: Off-Line Tests and Comparison with Other Schemes, J Climate, 28(3), 1268-1287 doi: 10.1175/Jcli-D-14-00102.1.

Gregory, D., and P. R. Rowntree (1990), A Mass Flux Convection Scheme with Representation of Cloud Ensemble Characteristics and Stability-Dependent Closure, Mon Weather Rev, 118(7), 1483-1506.

Haywood, J. M., and K. P. Shine (1995), The Effect of Anthropogenic Sulfate and Soot Aerosol on the Clear-Sky Planetary Radiation Budget, Geophys Res Lett, 22(5), 603-606 doi: Doi 10.1029/95gl00075.

Ilyina, T., K. D. Six, J. Segschneider, E. Maier-Reimer, H. M. Li, and I. Nunez-Riboni (2013), Global ocean biogeochemistry model HAMOCC: Model architecture and performance as component of the MPI-Earth system model in different CMIP5 experimental realizations, J Adv Model Earth Sy, 5(2), 287-315 doi: 10.1029/2012ms000178.

Jungclaus, J. H., N. Fischer, H. Haak, K. Lohmann, J. Marotzke, D. Matei, U. Mikolajewicz, D. Notz, and J. S. von Storch (2013), Characteristics of the ocean simulations in the Max Planck Institute Ocean Model (MPIOM) the ocean component of the MPI-Earth system model, J Adv Model Earth Sy, 5(2), 422-446 doi: 10.1002/jame.20023.

Khairoutdinov, M., and Y. Kogan (2000), A new cloud physics parameterization in a large-eddy simulation model of marine stratocumulus, Mon Weather Rev, 128(1), 229-243.

Kipling, Z., P. Stier, L. Labbouz, and T. Wagner (2017), Dynamic subgrid heterogeneity of convective cloud in a global model: description and evaluation of the Convective Cloud Field Model (CCFM) in ECHAM6-HAM2, Atmos. Chem. Phys., 17(1), 327-342 doi: 10.5194/acp-17-327-2017.

Kirkevåg, A., A. Grini, D. Olivié, Ø. Seland, K. Alterskjær, M. Hummel, I. H. Karset, A. Lewinschal, X. Liu, M. Schulz, and T. Iversen (2018), A production-tagged aerosol module for earth system models - extensions and updates for CAM5.3-Oslo, Geosci Model Dev, Submitted.

Labbouz, L., Z. Kipling, P. Stier, and A. Protat (2018), How Well Can We Represent the Spectrum of Convective Clouds in a Climate Model? Comparisons between Internal

Parameterization Variables and Radar Observations, Journal of the Atmospheric Sciences, 75, 1509-1524 doi: 10.1175/JAS-D-17-0191.s1.

Li, J. L. F., D. E. Waliser, G. Stephens, and S. Lee (2016), Characterizing and Understanding Cloud Ice and Radiation Budget Biases in Global Climate Models and Reanalysis, Meteor Mon, 56 doi: 10.1175/Amsmonographs-D-15-0007.1.

Lohmann, U., P. Stier, C. Hoose, S. Ferrachat, S. Kloster, E. Roeckner, and J. Zhang (2007), Cloud microphysics and aerosol indirect effects in the global climate model ECHAM5-HAM, Atmos. Chem. Phys., 7(13), 3425-3446 doi: DOI 10.5194/acp-7-3425-2007.

Malavelle, F. F., J. M. Haywood, A. Jones, A. Gettelman, L. Clarisse, S. Bauduin, R. P. Allan, I. H. H. Karset, J. E. Kristjansson, L. Oreopoulos, N. Cho, D. Lee, N. Bellouin, O. Boucher, D. P. Grosvenor, K. S. Carslaw, S.

Dhomse, G. W. Mann, A. Schmidt, H. Coe, M. E. Hartley, M. Dalvi, A. A. Hill, B. T. Johnson, C. E. Johnson, J. R. Knight, F. M. O'Connor, D. G. Partridge, P. Stier, G. Myhre, S. Platnick, G. L. Stephens, H. Takahashi, and T. Thordarson (2017), Strong constraints on aerosol-cloud interactions from volcanic eruptions (vol 546, pg 485, 2017), Nature, 551(7679), 256-256 doi: 10.1038/nature24275.

Mann, G. W., K. S. Carslaw, D. V. Spracklen, D. A. Ridley, P. T. Manktelow, M. P. Chipperfield, S. J. Pickering, and C. E. Johnson (2010), Description and evaluation of GLOMAP-mode: a modal global aerosol microphysics model for the UKCA composition-climate model, Geosci. Model Dev., 3, 519-551 doi: doi:10.5194/gmd-3-519-2010.

Morrison, H., and A. Gettelman (2008), A new two-moment bulk stratiform cloud microphysics scheme in the community atmosphere model, version 3 (CAM3). Part I: Description and numerical tests, J Climate, 21(15), 3642-3659 doi: Doi 10.1175/2008jcli2105.1.

Muller, C. J., and P. A. O'Gorman (2011), An energetic perspective on the regional response of precipitation to climate change, Nat Clim Change, 1(5), 266-271 doi: 10.1038/Nclimate1169.

Nordeng, T. E. (1994), Extended versions of the convective parameterization scheme at ECMWF and their impact on the mean and transient activity of the model in the tropics, 42 pp, ECMWF, Reading, UK.

Park, S., and C. S. Bretherton (2009), The University of Washington Shallow Convection and Moist Turbulence Schemes and Their Impact on Climate Simulations with the Community Atmosphere Model, J Climate, 22(12), 3449-3469 doi: 10.1175/2008jcli2557.1.

Quaas, J., Y. Ming, S. Menon, T. Takemura, M. Wang, J. E. Penner, A. Gettelman, U. Lohmann, N. Bellouin, O. Boucher, A. M. Sayer, G. E. Thomas, A. McComiskey, G. Feingold, C. Hoose, J. E. Kristjansson, X. Liu, Y. Balkanski, L. J. Donner, P. A. Ginoux, P. Stier, B. Grandey, J. Feichter, I. Sednev, S. E. Bauer, D. Koch, R. G. Grainger, A. Kirkevag, T. Iversen, O. Seland, R. Easter, S. J. Ghan, P. J. Rasch, H. Morrison, J. F. Lamarque, M. J. Iacono, S. Kinne, and M. Schulz (2009), Aerosol indirect effects - general circulation model intercomparison and evaluation with satellite data, Atmos. Chem. Phys., 9(22), 8697-8717 doi: 10.5194/acp-9-8697-2009.

Stevens, B., M. Giorgetta, M. Esch, T. Mauritsen, T. Crueger, S. Rast, M. Salzmann, H. Schmidt, J. Bader, K. Block, R. Brokopf, I. Fast, S. Kinne, L. Kornblueh, U. Lohmann, R. Pincus, T. Reichler, and E. Roeckner (2013), Atmospheric component of the MPI-M Earth System Model: ECHAM6, J Adv Model Earth Sy, 5(2), 146-172 doi: Doi 10.1002/Jame.20015.

Stier, P., J. Feichter, S. Kinne, S. Kloster, E. Vignati, J. Wilson, L. Ganzeveld, I. Tegen, M. Werner, Y. Balkanski, M. Schulz, O. Boucher, A. Minikin, and A. Petzold (2005), The aerosol-climate model ECHAM5-HAM, Atmos Chem Phys, 5, 1125-1156.

Stier, P., J. H. Seinfeld, S. Kinne, and O. Boucher (2007), Aerosol absorption and radiative forcing, Atmos Chem Phys, 7(19), 5237-5261.

Sundqvist, H., E. Berge, and J. E. Kristjansson (1989), Condensation and Cloud Parameterization Studies with a Mesoscale Numerical Weather Prediction Model, Mon Weather Rev, 117(8), 1641-1657 doi: Doi 10.1175/1520-0493(1989)117<1641:Cacpsw>2.0.Co;2.

Tegen, I., U. Lohmann, D. Neubauer, C. S.-L. Drian, S. Ferrachat, I. Bey, T. Stanelle, P. Stier, N. Schutgens, D. Watson-Parris, H. Schmidt, S. Rast, H. Kokkola, M. Schultz, S. Barthel, and B. Heinold (2018), The aerosol-climate model ECHAM6.3-HAM2.3: Aerosol evaluation, Geosci. Model Dev., in prep.

Tiedtke, M. (1989), A Comprehensive Mass Flux Scheme for Cumulus Parameterization in Large-Scale Models, Mon Weather Rev, 117(8), 1779-1800.

Vignati, E., J. Wilson, and P. Stier (2004), M7: An efficient size-resolved aerosol microphysics module for large-scale aerosol transport models, J Geophys Res-Atmos, 109(D22) doi: D22202, doi:10.1029/2003JD004485.

Wagner, T. M., and H. F. Graf (2010), An Ensemble Cumulus Convection Parameterization with Explicit Cloud Treatment, J. Atm. Sci., 67(12), 3854-3869 doi: 10.1175/2010jas3485.1.

Waliser, D. E., J. L. F. Li, C. P. Woods, R. T. Austin, J. Bacmeister, J. Chern, A. Del Genio, J. H. Jiang, Z. M. Kuang, H. Meng, P. Minnis, S. Platnick, W. B. Rossow, G. L. Stephens, S. Sun-Mack, W. K. Tao, A. M. Tompkins, D. G. Vane, C. Walker, and D. Wu (2009), Cloud ice: A climate model challenge with signs and expectations of progress, J Geophys Res-Atmos, 114 doi: Artn D00a21
10.1029/2008jd010015.

Zhang, G. J., and N. A. Mcfarlane (1995), Sensitivity of Climate Simulations to the Parameterization of Cumulus Convection in the Canadian Climate Center General-Circulation Model, Atmos Ocean, 33(3), 407-446 doi: Doi 10.1080/07055900.1995.9649539.

Zhang, K., D. O'Donnell, J. Kazil, P. Stier, S. Kinne, U. Lohmann, S. Ferrachat, B. Croft, J. Quaas, H. Wan, S. Rast, and J. Feichter (2012), The global aerosol-climate model ECHAM-HAM, version 2: sensitivity to improvements in process representations, Atmos. Chem. Phys., 12(19), 8911-8949 doi: 10.5194/acp-12-8911-2012.

6. Changes with respect to the DoW

Not applicable

7. Dissemination and uptake

Models assessed in this deliverable will be used for the assessment of terrestrial biosphere-atmosphere-cloud-climate interactions in Deliverable 4.4 as well as for future scenario simulations with three ESMs including an assessment (structure, contents) and of the role of future ship emissions with an ice-free Arctic ocean in Deliverable 4.5. Assessed BACCHUS ESMs will also contribute to experiments conducted under the current coupled model intercomparison project CMIP6 framework.